

Metal–Organic Frameworks

How to cite: *Angew. Chem. Int. Ed.* **2020**, *59*, 11349–11354

International Edition: doi.org/10.1002/anie.202003636

German Edition: doi.org/10.1002/ange.202003636

Rapid Generation of Hierarchically Porous Metal–Organic Frameworks through Laser Photolysis

Kun-Yu Wang, Liang Feng, Tian-Hao Yan, Shengxiang Wu, Elizabeth A. Joseph, and Hong-Cai Zhou*

Abstract: Hierarchically porous metal–organic frameworks (HP-MOFs) facilitate mass transfer due to mesoporosity while preserving the advantage of microporosity. This unique feature endows HP-MOFs with remarkable application potential in multiple fields. Recently, new methods such as linker labilization for the construction of HP-MOFs have emerged. To further enrich the synthetic toolkit of MOFs, we report a controlled photolytic removal of linkers to create mesopores within microporous MOFs at tens of milliseconds. Ultraviolet (UV) laser has been applied to eliminate “photolabile” linkers without affecting the overall crystallinity and integrity of the original framework. Presumably, the creation of mesopores can be attributed to the missing-cluster defects, which can be tuned through varying the time of laser exposure and ratio of photolabile/robust linkers. Upon laser exposure, MOF crystals shrank while metal oxide nanoparticles formed giving rise to the HP-MOFs. In addition, photolysis can also be utilized for the fabrication of complicated patterns with high precision, paving the way towards MOF lithography, which has enormous potential in sensing and catalysis.

Metal–organic frameworks (MOFs) are porous crystalline materials assembled using metal nodes and organic linkers.^[1] The last two decades has witnessed the burgeoning of MOFs as a promising candidate for various applications such as gas storage and separation, catalysis, and therapeutics.^[2] MOFs feature tailorable pore environments, which allow for incorporation of guest molecules and synergy of function groups.^[3] Nevertheless, most MOFs are microporous, which severely limits mass transfer within the framework.^[4,5] It is necessary but challenging to construct hierarchically porous MOFs (HP-MOFs) with access to the interior environment.^[6]

HP-MOFs can be constructed through reticular chemistry,^[7] templated synthesis^[8] and etching techniques.^[9] Zhou and co-workers have reported a linker labilization strategy, in which labile linkers are selectively eliminated in a multivariate MOF (MTV-MOF) to produce hierarchical pores.^[10] To date,

hydrolysis, thermolysis and ozonolysis have been reported to eliminate labile linkers selectively.^[10,11] Besides, the chemical environment of vacancies in MOFs can be modulated through a molecular wise approach.^[12] However, it is still a challenge to precisely control the size, shape and spatial arrangement of hierarchical pores, while ensuring the stability and integrity of HP-MOFs.

Laser, since its discovery in 1960, has changed human society in various fields such as metal processing, photolithography, surgery, astronomy and physics.^[13] Owing to its spatial coherence, lasers can focus high energy onto a defined area, allowing for applications like cutting, welding and even fabricating microscopic patterns.^[14] The utilization of laser in MOFs has recently been studied by Deng, Cheng and co-workers. Nanoscale laser metallurgy and patterning (nano-LaMP) was developed to convert MOFs to functional nanoparticles, including metals,^[15] transition-metal carbides^[16] and alloys,^[17] in which the metals and organic linkers could affect the light absorptivity and stability of MOFs and the complete conversion of some robust MOFs was challenging even at a high laser power.^[16] Presumably, through elaborate control of the laser and MOF compositions, the crystallinity and porosity, two representative properties of MOFs, can also be well preserved after photolysis, enabling feasibility for use in fabricating complicated architectures and composites based on this porous crystalline material. Herein, we report a controlled and rapid removal of linkers to create mesopores within microporous MOFs based upon laser photolysis. A 405 nm laser serves as the energy source to perform the photolysis, given the fact that photosensitive linkers within the MOF feature strong absorption at the wavelength of 405 nm. After photolysis, selective removal of photolabile linkers occurs at tens of milliseconds to generate a HP-MOF. Chemical bonds can be broken through simultaneous excitation of electrons or intensive heat generated by the laser, resulting in the removal of organic linkers and enlargement of MOF cavities. This is distinct from traditional cases using photosensitive MOFs in biological photothermal therapy, which does not involve the break of chemical bonds.^[18] In addition, this photolytic strategy can process local MOF particles in a highly controllable manner and fabricate complicated patterns on MOFs with a spatial resolution of approximate 40 micrometers.

UiO-66, a microporous robust MOF assembled by bicarbonate linkers BDC (BDC = 1,4-benzenedicarbonate) and $[\text{Zr}_6\text{O}_4(\text{OH})_4]$ clusters, was selected as the prototype for photolysis.^[19] A tetracarboxylate porphyrin linker TCPP (TCPP = tetrakis(4-carboxyphenyl)porphyrin) was incorporated into UiO-66, serving as the photolabile linker.^[20] The

[*] K.-Y. Wang, L. Feng, T.-H. Yan, S. Wu, E. A. Joseph, Prof. Dr. H.-C. Zhou
Department of Chemistry, Texas A&M University
College Station, TX 77843 (USA)
E-mail: zhou@chem.tamu.edu
Prof. Dr. H.-C. Zhou
Department of Materials Science and Engineering
Texas A&M University
College Station, TX 77842 (USA)

Supporting information and the ORCID identification number(s) for the author(s) of this article can be found under <https://doi.org/10.1002/anie.202003636>.

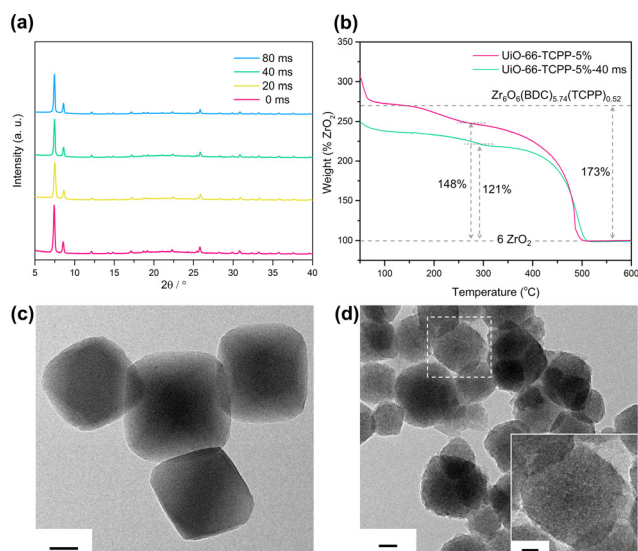


Figure 1. a) PXRD of UiO-66-TCPP-5%-time samples with various exposure time under laser. b) TGA of original UiO-66-TCPP-5% and UiO-66-TCPP-5%-40 ms samples. The top grey dash line refers to ideal defect-free UiO-66-TCPP-5%. c) TEM image of as-synthesized UiO-66-TCPP-5% particles. The scale bar is 50 nm. d) TEM image of UiO-66-TCPP-5%-40 ms particles. Scale bars are 50 nm in (c,d), and 100 nm in the insert image.

photolysis was performed using a homemade laser system equipped with a continuous 405 nm laser. Due to the robustness of BDC linkers, laser treatment on pristine UiO-66 could not induce the formation of hierarchical pores (Figure 2a). The incorporation of photolabile linkers as sacrificing templates is very necessary to create defects in MTV-MOFs (Figure 2b). In a typical photolytic process, an activated UiO-66-TCPP-5% sample was exposed to the UV laser with a measured real-time intensity of $7 \times 10^7 \text{ W m}^{-2}$. The residence

time of individual laser spots could be tuned at a millisecond level. The pristine UiO-66-TCPP-5% featured a type I isotherm in N_2 sorption test at 77 K, indicating the presence of micropores. Once exposed to laser for 20 ms or 40 ms, an increase in BET surface area and mesopores was observed (Figure 3a). Pore size distribution demonstrated that mesopores around 3 nm appeared after laser treatment, which can be attributed to the missing-cluster defects, and the ratio of mesopore/micropore increased with elongated exposure time (Figures 3b,c). Considering the photolytic process was performed in the solid phase, as-formed residues might be trapped in the pores, resulting in a reduction in observed porosity and pore width in the MOF. Thus, a DMF solution containing 0.1% HCl was applied to wash the sample and remove residues. After washing with the diluted acid, the BET surface areas of the laser-treated sample increased and an accompanying rise in enlarged mesopores could also be observed (Figures 3d,e). As indicated by PXRD, the crystallinity of the MOF sample was still maintained after laser exposure (Figure 1a), indicating that the photolytic method could preserve the stability and integrity of the MOF. $^1\text{H NMR}$ measurement of digested samples demonstrated that the ratio of TCPP/BDC in the MOF decreased after a longer exposure time (Table S2).

Besides exposure time, the proportion of photolabile ligands is also a factor that can be utilized to further augment the mesopore ratio. However, the ratio TCPP/BDC in UiO-66 is restricted by the synthetic conditions, and too much TCPP, as a tetracarboxylate linker, will result in non-homogeneous phases. Therefore, other ligands with potentially photolytic properties have been explored. It was found that BDC-NH₂ could be an appropriate candidate for two reasons. Firstly, BDC-NH₂ could be combined with BDC at any ratio to afford well-mixed MTV-UiO-66 without forming other MOF species. Secondly, UiO-66-NH₂, a MOF fabricated by $[\text{Zr}_6\text{O}_4-$

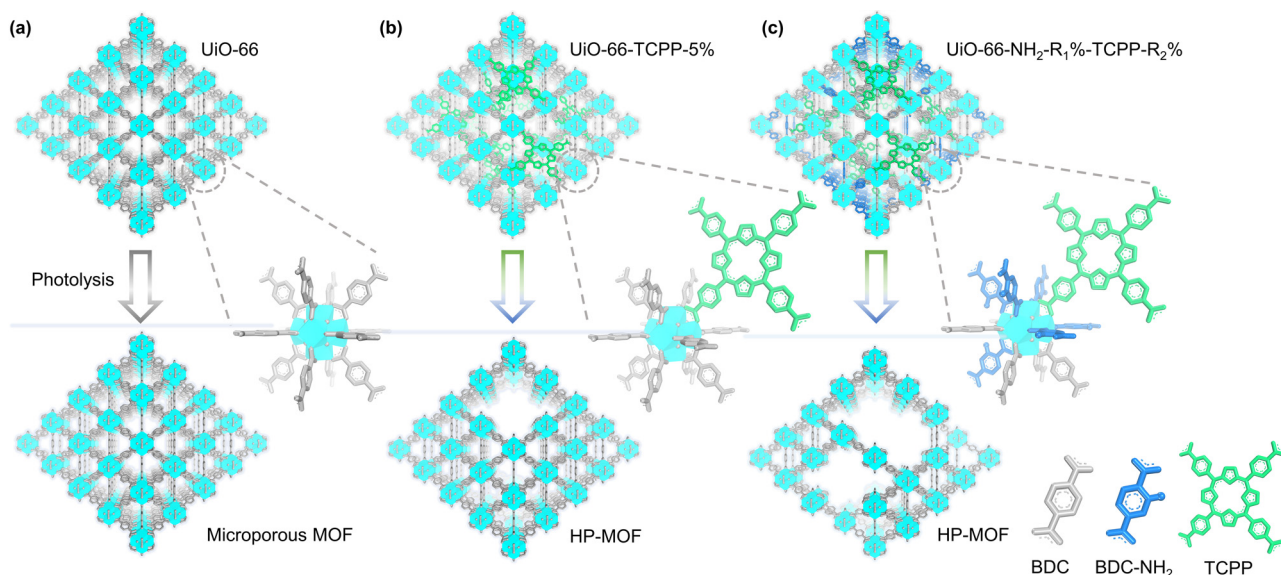


Figure 2. a) Microporosity and integrity of UiO-66 are preserved after photolysis. b) Photolysis on UiO-66-TCPP-5% can generate mesopores through eliminating the photolabile linker TCPP. c) Introducing a secondary labile linker BDC-NH₂ can increase the ratio of mesopores to micropores after photolysis. The Zr atoms are represented as cyan polyhedra and H atoms are omitted for clarification.

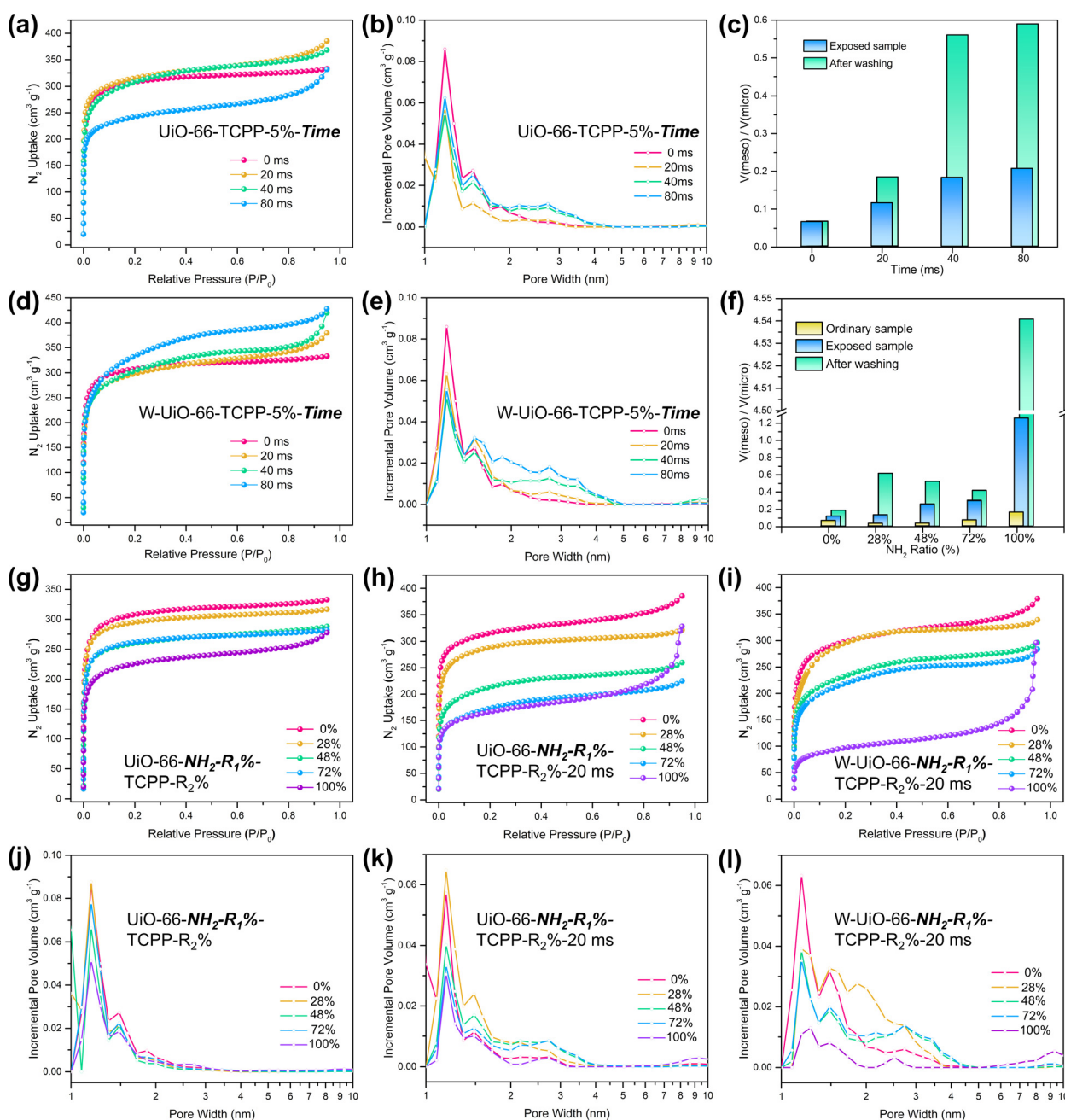


Figure 3. N_2 sorption isotherms and pore size distributions of UiO-66-TCPP-5% samples with various exposed time under laser (a,b), UiO-66-TCPP-5%-time samples washed with diluted acid solution (d,e), as-synthesized UiO-66- NH_2 - R_1 %-TCPP- R_2 % samples (g,i), UiO-66- NH_2 - R_1 %-TCPP- R_2 % samples treated with laser for 20 ms (h,k), and UiO-66- NH_2 - R_1 %-TCPP- R_2 %-20 ms samples after washing in diluted acid solution (i,l). Meso- to micropore volume ratio of UiO-66-TCPP-5%-time samples before and after washing (c) and UiO-66- NH_2 - R_1 %-TCPP- R_2 % samples before and after washing (f). A density functional theory (DFT) model was applied to calculate the pore size distributions of the MOF samples according to the N_2 adsorption isotherms.

(OH)₄ cluster and BDC-NH₂, is less stable under 405 nm laser compared with the ordinary UiO-66 (Figure S34). However, photolysis on UiO-66-NH₂ was not successful because the BET surface area plummeted after laser exposure while the ratio of as-formed mesopores was limited. To solve this dilemma, BDC-NH₂ can be incorporated into the UiO-66-TCPP to attain a ternary MTV-UiO-66, which imparts more lability to the framework (Figure 2c). Thus, a series of microporous ternary UiO-66- NH_2 - R_1 %-TCPP- R_2 %

with various linker ratios were synthesized following the stepwise strategy as mentioned. Once exposed to the 405 nm laser for 20 ms, BET surface areas of these ternary MOFs dropped while the ratio of mesopores increased (Figures 3 f,h,k). Subsequently, more mesopores were generated after washing, ranging from 2 nm to 4.5 nm, exceeding the performance of laser-treated binary UiO-66-TCPP, further confirming the synergistic effect between the two photolabile linkers. Interestingly, ¹H NMR measurement on the digested

ternary MOF revealed an obvious decrease in the BDC-NH₂ ratio (Table S3). Owing to its lability and high proportion, the change in BDC-NH₂ amount is easier to be noticed compared with the minor TCPP linker as well as the stable BDC linker.

According to transmission electron microscope (TEM) images, the surface of hierarchically porous UiO-66 MOFs became uneven after photolysis (Figure 1). Additionally, ultra-small ZrO₂ nanoparticles, showing lattice fringes with 0.295 nm lattice spacing of [101] planes, were observed, indicating the cluster aggregation phenomenon after photolysis (Figure S13).

Remarkably, photolysis of MOFs can be precisely controlled in both time and spatial scales to result in complicated patterns. For instance, during photolysis of UiO-66-TCPP-5% powder, the untreated MOF sample adopted a garnet color, which would change to greenish-brown after photolysis (Figures 4a,b). A color difference could also be observed under a 362 nm UV lamp, indicating decomposition of porphyrin ligands (Figure 4c). With a spatial resolution of $\approx 40 \mu\text{m}$ (Figures 4e,f,g), diverse patterns such as well-known

artworks could be depicted on MOF powders via laser photolithography (Figures 4g,h,i). The essential factor is the coherence of laser, which allows for precise processing in a confined region without interrupting the surrounding structure. This unique merit provides a top-down approach to align two distinct MOF particles into a designed array with application potentials in catalysis and recognition.^[21]

We propose a photothermal mechanism to account for the generation of mesopores inside UiO-66-TCPP (Figures 4d, S13). Photothermal effects of MOFs, which have been widely applied in catalysis, guest release and bio-application, involve photon absorption and excitation of electrons.^[22] When the excited electrons return to the ground state, heat or light can be generated. In the UiO-66-TCPP system, the doped photosensitive TCPP linkers are initially appended to missing-linker defects, where carboxylates of a TCPP linker are coordinated to the Zr-oxo cluster presumably. Once exposed to the 405 nm laser, the conjugated porphyrin ring in TCPP linker can absorb photon and generate elevated temperatures in a local domain, leading to decomposition of adjacent

linkers and aggregation of clusters. It should be noted that the break of chemical bonds in the laser photolysis can be triggered by simultaneous excitation of electrons or intense heat within the framework, and further mechanism study is required. The well-mixed distribution of TCPP linkers rules out the possibility of forming large mesopores inside UiO-66. In the case of nano-LaMP, the laser can deliver concentrated energy to the secondary building units and generate high temperature evenly across the crystal.^[16] While the nano-LaMP usually destroys the framework thoroughly and converts MOFs into nanoparticles, the laser photolysis in this work can selectively eliminate photosensitive linkers to generate a partially decomposed MOF featuring hierarchical porosity. In addition, according to the UV-vis spectroscopy, strong absorption peaks around 405 nm were observed in TCPP and BDC-NH₂, except for BDC, which accounted for the selectivity of laser

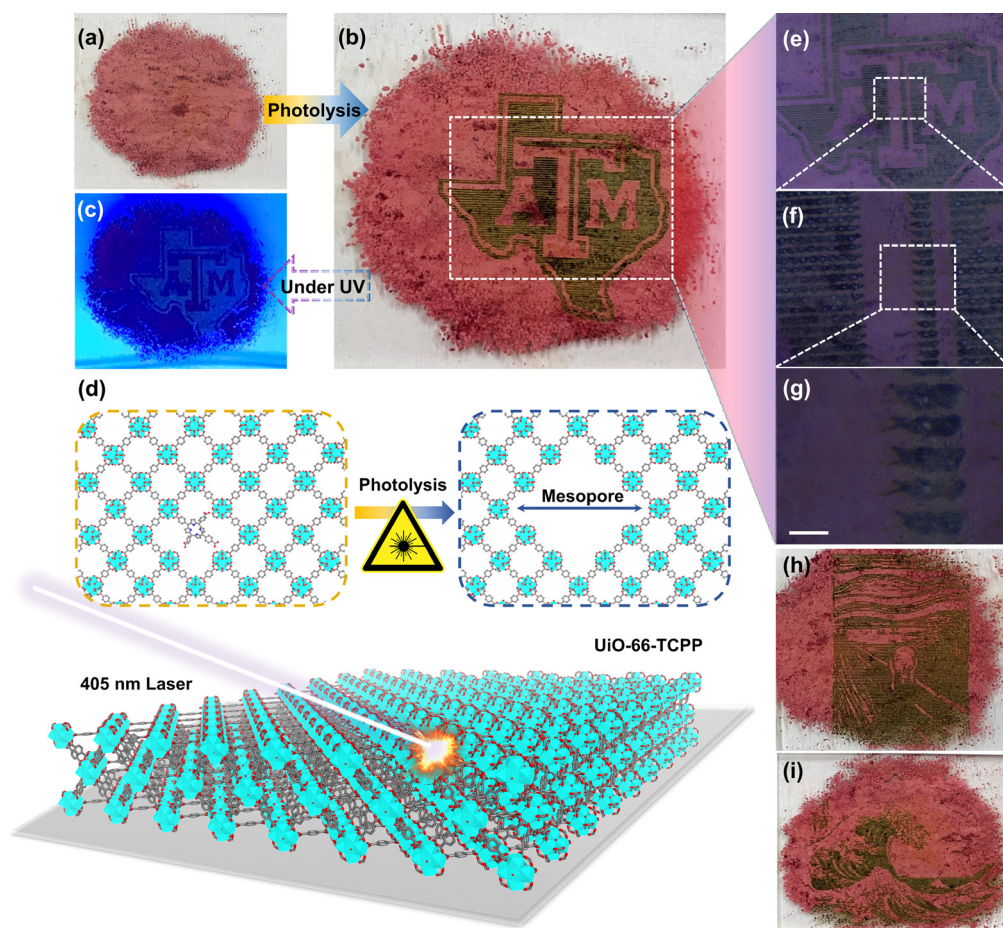


Figure 4. a) Optical photograph of original UiO-66-TCPP-5% powders. b) Optical photograph of Texas A&M University's logo on UiO-66-TCPP-5% powders after programmable photolithography. The exposure time for each spot is 40 ms. c) Optical photograph of the patterned MOF sample under UV lamp. e,f,g) Microscopic photograph of details in the patterned UiO-66-TCPP-5% powders. The scale bar is 50 μm . h,i) Artworks *The Scream* and *The Great Wave off Kanagawa* fabricated via programmable photolithography. d) The experimental process of photolysis on UiO-66-TCPP. The cyan polyhedra represent Zr atoms and H atoms are omitted for clarification. O, C and N atoms are represented in red, grey and blue, respectively.

photolysis (Figure S14). The mechanism of linker photolysis was further elucidated through infrared (IR) spectroscopy, thermogravimetry analysis (TGA) and ^1H NMR spectroscopy. IR spectroscopy of photolyzed UiO-66-TCPP MOFs with varying periods of exposure to the UV source, including 20, 40 and 80 ms, shows the decrease of peaks at around 3428 cm^{-1} associated with $\nu(\text{N-H})$ on porphyrin rings, indicating the partial decomposition of TCPP linkers in MTV-MOFs (Figure S9). Additionally, the decarboxylation process was observed after photolysis, as evidenced by a slight shift and loss of the carboxylate bands ($1576, 1428, 1392\text{ cm}^{-1}$). The composition of UiO-66-TCPP-5% before and after photolysis was further analyzed by TGA (Figure 1b). Notably, UiO-66-TCPP-5%-40 ms shows lower weight loss than UiO-66-TCPP-5% during linker decomposition stages, due to the partial loss of organic linkers during photolysis. In addition, by using porphyrin MOF PCN-224 for comparison, the photolytic degradation of TCPP was investigated through Raman scattering spectrum and ^1H NMR. After 80 ms exposure under laser, D band and G band arose in PCN-224 according to Raman spectra, indicating generation of defective graphite (Figure S10). ^1H NMR spectra demonstrated decarboxylation and oxidative destruction of the porphyrin linker, resulting in diphenyl ether and its derivatives (Figures S11, S12).

To further study whether linker photolysis can be extended to other MOF systems, we selected another photosensitive linker cobalt tetra(carboxy)phthalocyanine (CoPc) as the labile linkers to construct MTV-MOFs. Following a similar procedure, mixed-linker UiO-66-CoPc was prepared through one-pot synthesis. After laser treatment for 20 ms, mesopores were formed while the overall crystallinity was maintained, as indicated by the N_2 sorption isotherms and PXRD patterns (Figures S18, S19). We also explored the versatility of linker photolysis in MTV-MOFs with various metal nodes and organic linkers, such as UiO-66-Cu-TCPP, UiO-66-Co-TCPP, ZIF-8(Zn)-TCPP, UiO-67-TCPP, and UiO-66(Hf)-TCPP. From the N_2 sorption isotherms, it was determined that mesopores in these MTV-MOFs were generated as a result of the laser treatment (Figures S16–S28).

Furthermore, we have shown that selective engineer on hierarchical MOF-on-MOF structures could be achieved by photolysis. As a proof of concept, we incorporated nanosized PCN-224 into the lattice of large MOF-5 crystals. Selective decomposition of core PCN-224 MOFs was achieved in PCN-224@MOF-5 after laser treatment, as indicated by the color change from purple to brown from optical images (Figures 5a,b). Meanwhile, the colorless MOF-5 shell was preserved, as confirmed by both PXRD patterns and optical images (Figure S29). Similarly, this controlled formation of hierarchical structures could also be achieved in hierarchical PCN-224@ZIF-8 structures, demonstrating the feasibility of photolysis in engineering hierarchical MOF structures (Figures S31–S33).

Overall, we report a versatile and effective strategy to generate hierarchically porous MOFs through laser photolysis. Compared with reported linker labilization strategies such as hydrolysis, thermolysis and ozonolysis, the laser photolysis exhibits merits in terms of spatial resolution,

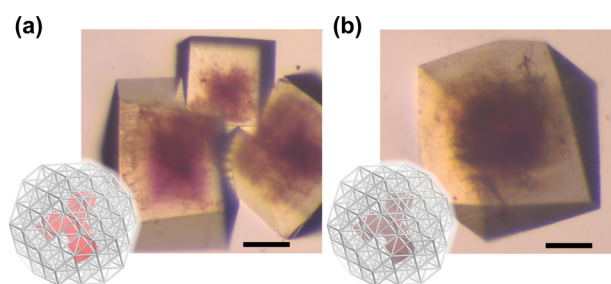


Figure 5. a) Microscopic photograph of MOF-5@PCN-224. The scale bar is $100\ \mu\text{m}$. b) Microscopic photograph of MOF-5@PCN-224 after 1 s laser exposure. The scale bar is $100\ \mu\text{m}$.

fabrication speed, power consumption and cost (Figure S39). Besides, the structural integrity of mixed-linker MOFs can be maintained after laser photolysis. This method is expected to engineer hierarchical MOF structures and produce complicated MOF patterns for cascade reactions and recognition. Further detailed studies on photolytic mechanism through spectroscopy and simulation are currently in progress in our lab.

Acknowledgements

This research was supported as part of the Center for Gas Separations, an Energy Frontier Research Center funded by the U.S. Department of Energy, Office of Science, Basic Energy Sciences under Award Number DE-SC0001015, the Robert A. Welch Foundation through a Welch Endowed Chair to H.-C.Z. (A-0030). The authors also acknowledge the financial supports of Qatar National Research Fund under Award Number NPRP9-377-1-080.

Conflict of interest

The authors declare no conflict of interest.

Keywords: hierarchical pores · linker photolysis · metal–organic frameworks

- [1] H. C. Zhou, J. R. Long, O. M. Yaghi, *Chem. Rev.* **2012**, *112*, 673–674.
- [2] a) J. R. Li, R. J. Kuppler, H. C. Zhou, *Chem. Soc. Rev.* **2009**, *38*, 1477–1504; b) J. Lee, O. K. Farha, J. Roberts, K. A. Scheidt, S. T. Nguyen, J. T. Hupp, *Chem. Soc. Rev.* **2009**, *38*, 1450–1459; c) M. X. Wu, Y. W. Yang, *Adv. Mater.* **2017**, *29*, 1606134.
- [3] a) M. Eddaoudi, J. Kim, N. Rosi, D. Vodak, J. Wachter, M. O’Keeffe, O. M. Yaghi, *Science* **2002**, *295*, 469–472; b) L. Feng, K. Y. Wang, G. S. Day, H. C. Zhou, *Chem. Soc. Rev.* **2019**, *48*, 4823–4853; c) M. Li, D. Li, M. O’Keeffe, O. M. Yaghi, *Chem. Rev.* **2014**, *114*, 1343–1370; d) W. Lu, Z. Wei, Z. Y. Gu, T. F. Liu, J. Park, J. Park, J. Tian, M. Zhang, Q. Zhang, T. Gentle 3rd, M. Bosch, H. C. Zhou, *Chem. Soc. Rev.* **2014**, *43*, 5561–5593; e) N. Stock, S. Biswas, *Chem. Rev.* **2012**, *112*, 933–969.
- [4] A. J. Howarth, Y. Y. Liu, P. Li, Z. Y. Li, T. C. Wang, J. Hupp, O. K. Farha, *Nat. Rev. Mater.* **2016**, *1*, 15018.

- [5] P. Li, J. A. Modica, A. J. Howarth, E. L. Vargas, P. Z. Moghadam, R. Q. Snurr, M. Mrksich, J. T. Hupp, O. K. Farha, *Chem* **2016**, *1*, 154–169.
- [6] Y. Luo, M. Ahmad, A. Schug, M. J. A. M. Tsotsalas, *Adv. Mater.* **2019**, *31*, 1901744.
- [7] a) D. W. Feng, Z. Y. Gu, J. R. Li, H. L. Jiang, Z. W. Wei, H. C. Zhou, *Angew. Chem. Int. Ed.* **2012**, *51*, 10307–10310; *Angew. Chem.* **2012**, *124*, 10453–10456; b) J. E. Mondloch, W. Bury, D. Fairen-Jimenez, S. Kwon, E. J. DeMarco, M. H. Weston, A. A. Sarjeant, S. T. Nguyen, P. C. Stair, R. Q. Snurr, O. K. Farha, J. T. Hupp, *J. Am. Chem. Soc.* **2013**, *135*, 10294–10297.
- [8] a) L. B. Sun, J. R. Li, J. Park, H. C. Zhou, *J. Am. Chem. Soc.* **2012**, *134*, 126–129; b) L. G. Qiu, T. Xu, Z. Q. Li, W. Wang, Y. Wu, X. Jiang, X. Y. Tian, L. D. Zhang, *Angew. Chem. Int. Ed.* **2008**, *47*, 9487–9491; *Angew. Chem.* **2008**, *120*, 9629–9633; c) Y. J. Zhao, J. L. Zhang, B. X. Han, J. L. Song, J. S. Li, Q. A. Wang, *Angew. Chem. Int. Ed.* **2011**, *50*, 636–639; *Angew. Chem.* **2011**, *123*, 662–665; d) S. Cao, G. Gody, W. Zhao, S. Perrier, X. Y. Peng, C. Ducati, D. Y. Zhao, A. K. Cheetham, *Chem. Sci.* **2013**, *4*, 3573–3577; e) G. R. Cai, H. L. Jiang, *Angew. Chem. Int. Ed.* **2017**, *56*, 563–567; *Angew. Chem.* **2017**, *129*, 578–582; f) H. L. Huang, J. R. Li, K. K. Wang, T. T. Han, M. M. Tong, L. S. Li, Y. B. Xie, Q. Y. Yang, D. H. Liu, C. L. Zhong, *Nat. Commun.* **2015**, *6*, 8847; g) L. H. Wee, C. Wiktor, S. Turner, W. Vanderlinden, N. Janssens, S. R. Bajpe, K. Houthoofd, G. Van Tendeloo, S. De Feyter, C. E. A. Kirschhock, J. A. Martens, *J. Am. Chem. Soc.* **2012**, *134*, 10911–10919.
- [9] a) Y. Kim, T. Yang, G. Yun, M. B. Ghasemian, J. Koo, E. Lee, S. J. Cho, K. Kim, *Angew. Chem. Int. Ed.* **2015**, *54*, 13273–13278; *Angew. Chem.* **2015**, *127*, 13471–13476; b) J. Koo, I. C. Hwang, X. Yu, S. Saha, Y. Kim, K. Kim, *Chem. Sci.* **2017**, *8*, 6799–6803; c) P. F. Yang, F. X. Mao, Y. S. Li, Q. X. Zhuang, J. L. Gu, *Chem. Eur. J.* **2018**, *24*, 2962–2970; d) M. Hu, Y. Ju, K. Liang, T. Suma, J. W. Cui, F. Caruso, *Adv. Funct. Mater.* **2016**, *26*, 5827–5834.
- [10] S. Yuan, L. F. Zou, J. S. Qin, J. L. Li, L. Huang, L. A. Feng, X. A. Wang, M. Bosch, A. Alsalmé, T. Cagin, H. C. Zhou, *Nat. Commun.* **2017**, *8*, 15356.
- [11] a) L. Feng, S. Yuan, L. L. Zhang, K. Tan, J. L. Li, A. Kirchon, L. M. Liu, P. Zhang, Y. Han, Y. J. Chabal, H. C. Zhou, *J. Am. Chem. Soc.* **2018**, *140*, 2363–2372; b) V. Guillerm, H. Xu, J. Albalad, I. Imaz, D. MasPOCH, *J. Am. Chem. Soc.* **2018**, *140*, 15022–15030.
- [12] Y. Wang, Q. Liu, Q. Zhang, B. Peng, H. X. Deng, *Angew. Chem. Int. Ed.* **2018**, *57*, 7120–7125; *Angew. Chem.* **2018**, *130*, 7238–7243.
- [13] L. R. Meza, S. Das, J. R. J. S. Greer, *Science* **2014**, *345*, 1322–1326.
- [14] a) R. K. Deshpande, G. I. Waterhouse, G. B. Jameson, S. G. Telfer, *Chem. Commun.* **2012**, *48*, 1574–1576; b) J. J. Yan, J. C. MacDonald, A. R. Maag, F. X. Coudert, S. C. Burdette, *Chem. Eur. J.* **2019**, *25*, 8393–8400.
- [15] H. Q. Jiang, S. Y. Jin, C. Wang, R. Q. Ma, Y. Y. Song, M. Y. Gao, X. T. Liu, A. G. Shen, G. J. Cheng, H. X. Deng, *J. Am. Chem. Soc.* **2019**, *141*, 5481–5489.
- [16] Y. S. Wu, Z. Huang, H. Q. Jiang, C. Wang, Y. Zhou, W. Shen, H. L. Xu, H. X. Deng, *ACS Appl. Mater. Interfaces* **2019**, *11*, 44573–44581.
- [17] W. Zhang, W. Yan, H. Q. Jiang, C. Wang, Y. Zhou, F. H. Ke, H. J. Cong, H. X. Deng, *ACS Sustainable Chem. Eng.* **2020**, *8*, 335–342.
- [18] G. Lan, K. Ni, W. Lin, *Coord. Chem. Rev.* **2019**, *379*, 65–81.
- [19] J. H. Cavka, S. Jakobsen, U. Olsbye, N. Guillou, C. Lamberti, S. Bordiga, K. P. Lillerud, *J. Am. Chem. Soc.* **2008**, *130*, 13850–13851.
- [20] Y. J. Sun, L. X. Sun, D. W. Feng, H. C. Zhou, *Angew. Chem. Int. Ed.* **2016**, *55*, 6471–6475; *Angew. Chem.* **2016**, *128*, 6581–6585.
- [21] a) G. R. Cai, W. Zhang, L. Jiao, S. H. Yu, H. L. Jiang, *Chem* **2017**, *2*, 791–802; b) J. J. Duan, S. Chen, C. Zhao, *Nat. Commun.* **2017**, *8*, 15341; c) I. Stassen, N. C. Burtch, A. A. Talin, P. Falcaro, M. D. Allendorf, R. Ameloot, *Chem. Soc. Rev.* **2017**, *46*, 3185–3241.
- [22] a) Y. Z. Chen, Z. U. Wang, H. W. Wang, J. L. Lu, S. H. Yu, H. L. Jiang, *J. Am. Chem. Soc.* **2017**, *139*, 2035–2044; b) L. Feng, S. Yuan, J. L. Li, K. Y. Wang, G. S. Day, P. Zhang, Y. Wang, H. C. Zhou, *ACS Cent. Sci.* **2018**, *4*, 1719–1726; c) J. Espín, L. Garzon-Tovar, A. Carné-Sánchez, I. Imaz, D. MasPOCH, *ACS Appl. Mater. Interfaces* **2018**, *10*, 9555–9562; d) J. D. Xiao, H. L. Jiang, *Acc. Chem. Res.* **2019**, *52*, 356–366; e) B. Z. Lu, Y. F. Chen, P. Y. Li, B. Wang, K. Mullen, M. Z. Yin, *Nat. Commun.* **2019**, *10*, 767; f) K. Zhang, X. D. Meng, Y. Cao, Z. Yang, H. F. Dong, Y. D. Zhang, H. T. Lu, Z. J. Shi, X. J. Zhang, *Adv. Funct. Mater.* **2018**, *28*, 1804634.

Manuscript received: March 10, 2020

Revised manuscript received: April 3, 2020

Accepted manuscript online: April 3, 2020

Version of record online: May 11, 2020